Journal of Alloys and Compounds 509 (2011) 7985–7992

Contents lists available at ScienceDirect

Journal of Alloys and Compounds

journal homepage: www.elsevier.com/locate/jallcom

Synthesis and electrochemical performance of $Li(Ni_{0.8}Co_{0.15}Al_{0.05})_{0.8}(Ni_{0.5}Mn_{0.5})_{0.2}O_2$ with core–shell structure as cathode material for Li-ion batteries

Jeong-Hun Ju, Kwang-Sun Ryu *

Department of Chemistry, University of Ulsan, Daehak-ro 93, Nam-gu, Ulsan 680-749, Republic of Korea

ARTICLE INFO

Article history:
Received 21 July 2010
Received in revised form 15 May 2011
Accepted 16 May 2011
Available online 23 May 2011

Keywords:
Lithium ion batteries
Cathode
$LiNi_{0.8}Co_{0.15}Al_{0.05}O_2$
$LiNi_{0.5}Mn_{0.5}O_2$
Core–shell
Co-precipitation

ABSTRACT

The core–shell structure cathode material $Li(Ni_{0.8}Co_{0.15}Al_{0.05})_{0.8}(Ni_{0.5}Mn_{0.5})_{0.2}O_2$ (LNCANMO) was synthesized via a co-precipitation method. Its applicability as a cathode material for lithium ion batteries was investigated. The core–shell particle consists of $LiNi_{0.8}Co_{0.15}Al_{0.05}O_2$ (LNCAO) as the core and a $LiNi_{0.5}Mn_{0.5}O_2$ as the shell. The thickness of the $LiNi_{0.5}Mn_{0.5}O_2$ layer is approximately 1.25 μm, as estimated by field emission scanning electron microscopy (FE-SEM). The cycling behavior between 2.8 and 4.3 V at a current rate of 18 mA g^{-1} shows a reversible capacity of about 195 mAh g^{-1} with little capacity loss after 50 cycles. High-rate capability testing shows that even at a rate of 5 C, a stable capacity of approximately 127 mAh g^{-1} is retained. In contrast, the capacity of LNCAO rapidly decreases in cyclic and high rate tests. The observed higher current rate capability and cycle stability of LNCANMO can be attributed to the lower impedance including charge transfer resistance and surface film resistance. Differential scanning calorimetry (DSC) indicates that LNCANMO had a much improved oxygen evolution onset temperature of approximately 251 °C, and a much lower level of exothermic-heat release compared to LNCAO. The improved thermal stability of the LNCANMO can be ascribed to the thermally stable outer shell of $LiNi_{0.5}Mn_{0.5}O_2$, which suppresses oxygen release from the host lattice and not directly come into contact with the electrolyte solution. In particular, LNCANMO is shown to exhibit improved electrochemical performance and is a safe material for use as an electrode for lithium ion batteries.

1. Introduction

Recent research has focused on the development and application of large-scale lithium ion batteries for hybrid and fully electric vehicles. Although high power and high energy are desirable performance characteristics, the issue of safety is one of the most important considerations in these applications. The thermal stability of lithium storage materials in the presence and absence of electrolytes plays an important role in determining the safety characteristics of lithium batteries. $LiNiO_2$ is a more attractive material than $LiCoO_2$ because of the low cost of fabrication and the possibility of higher rechargeable capacity. Nevertheless, this material possesses several disadvantages such as low-thermal instability and surface transformation resulting from the reaction with the electrolyte during cycling [1–3]. To address these shortcomings, $LiNi_{1-x}Co_xO_2$ ($0 < x < 1$) compounds have been developed motivated in part by the fact that $LiCoO_2$ and $LiNiO_2$ have the same layered α-$NaFeO_2$ structure [4–6]. Elements such as Al [7,8], Cr [9], Fe [10], Ga [11], Mg [12], Sn [13], Sr [14], Ti [15], and Zn [16] have been used for partial substitution of Ni or Co to further enhance the electrochemical performance of the $LiNi_{0.8}Co_{0.2}O_2$, which is a promising cathode material among these compounds. Lee et al. have reported that Al doped Co substituted Li nickelate cathode material, $LiNi_{0.85}Co_{0.10}Al_{0.05}O_2$, showed enhanced electrochemical properties and good thermal stability compared with $LiNiO_2$ and $LiNi_{0.85}Co_{0.10}Fe_{0.05}O_2$ [17]. Al-doping is particularly useful because Al ions are electrochemically inactive during the cycling process, and the strong Al–O bonds help in stabilizing the layered structure. Al-doping may also improve the discharge voltage [18]. Yoon et al. have reported good electrochemical properties of $LiNi_{0.8}Co_{0.15}Al_{0.05}O_2$ cathode materials such as high capacity (190 mAh g^{-1} at 0.1 C rates), good rate performance (capacity at 2 C rate retained to 88% of 0.1 C capacity), and good cycling performance (almost no capacity fading up to 40 cycles) [19]. The substitution of Ni by Co and by Al improves the structural stability of the oxide, but the thermal instability of $Li_{1-\delta}(Ni_{1-x-y}Co_xAl_y)O_2$ still remains an issue. It has been reported that commercial Li-ion cells using a $Li_{1-\delta}(Ni_{1-x-y}Co_xAl_y)O_2$ cathode suffer violent thermal runaway at approximately 210 °C [18,20,21].

* Corresponding author. Tel.: +82 522592763; fax: +82 522592 348.
E-mail address: ryuks@ulsan.ac.kr (K.-S. Ryu).

0925-8388/$ – see front matter © 2011 Elsevier B.V. All rights reserved.
doi:10.1016/j.jallcom.2011.05.060

Table 1
Comparison of structure parameters of LNCAO and LNCANMO.

Samples	a (Å)	c (Å)	c/a	I_{003}/I_{104}	R factor	Volume (Å^3)
LNCAO	2.8690(6)	14.1985(8)	4.949	1.25	0.16	101.217
LNCANMO	2.8720(4)	14.2120(8)	4.948	1.29	0.16	101.524

Ohzuku and Makimura [22] proposed the layered $LiNi_{0.5}Mn_{0.5}O_2$ material, showing a reversible capacity of 150 mAh g^{-1} in the voltage range of 2.5–4.3 V, to overcome the disadvantages of lithium transition metal oxides e.g., $LiNiO_2$ and $LiMnO_2$ [23]. $LiNi_{0.5}Mn_{0.5}O_2$ is a layered material that is isostructural with α-$NaFeO_2$, which consists of a closely packed network of oxygen atoms with Li^+ ions and transition metal ions (Ni^{2+} and Mn^{4+}) ordering of alternating planes of cubic structure. The electronic structure of Ni ions in $LiNi_{0.5}Mn_{0.5}O_2$ is unique: $Ni^{3+}(t_{2g}^6e_g^1)$ in $LiNiO_2$ becomes $Ni^{2+}(t_{2g}^6e_g^2)$ upon substitution of $Mn^{4+}(t_{2g}^3e_g^0)$. Lithium removal from $LiNi^{2+}_{0.5}Mn^{4+}_{0.5}O_2$ is accompanied by the oxidation of Ni^{2+} to Ni^{4+} via Ni^{3+} while Mn^{4+} remains electrochemically inactive [24–30]. The onset of the exothermal temperature of deeply delithiated $Li_{1-x}(Ni_{0.5}Mn_{0.5})O_2$ is observed usually as high as 280 °C. Heat generation at this temperature is significantly reduced relative to Ni-rich $Li_{1-\delta}(Ni_{1-x-y}Co_xAl_y)O_2$ [18,20,21,31,32]. For delithiation, the decrease in the cell volume in this material is smaller (~3%) [33] in contrast to the large decrease in the cell volume observed for other transition metal oxides such as $LiNiO_2$ (~10%), $LiMnO_2$ (~8%), and $LiCoO_2$ (~6%). This electrochemical structure and the relatively small change in the cell volume are extremely beneficial with respect to the cycling stability, cell life, rate capability, and thermal stability of the batteries produced using these materials.

To take high capacity of Ni-rich $Li[Ni_{1-x}M_x]O_2$ (M = Metal) and thermal stability of $LiNi_{0.5}Mn_{0.5}O_2$, Sun et al. applied core–shell materials to $Li(Ni_{0.8}Co_{0.1}Mn_{0.1})_{0.8}(Ni_{0.5}Mn_{0.5})_{0.2}O_2$ and Li $(Ni_{0.8}Co_{0.2})_{0.8}(Ni_{0.5}Mn_{0.5})_{0.2}O_2$ system [34,35]. In case of $Li(Ni_{0.8}Co_{0.1}Mn_{0.1})_{0.8}(Ni_{0.5}Mn_{0.5})_{0.2}O_2$ system, considerable capacity retention of 98% after 500 cycles and thermal stability (the exothermic temperature of about 250 °C) were observed in $Li(Ni_{0.8}Co_{0.1}Mn_{0.1})_{0.8}(Ni_{0.5}Mn_{0.5})_{0.2}O_2$. Also, they have reported the electrochemical properties and thermal stability of all layered transition metal oxide, $Li(Ni_{1/3}Co_{1/3}Mn_{1/3})O_2$, core and $LiNi_{0.5}Mn_{0.5}O_2$ material [36]. However, it is expected that the use of Al doped Co substituted Li nickelate core material, $LiNi_{0.85}Co_{0.10}Al_{0.05}O_2$, may lead to better electrochemical properties and good thermal stability compared with the core materials mentioned above. In this study, we have designed a spherical core–shell material: $LiNi_{0.8}Co_{0.15}Al_{0.05}O_2$ (LNCAO) as the core which can deliver a high capacity of 200 mAh g^{-1}, and $LiNi_{0.5}Mn_{0.5}O_2$ as the shell which can provide the significant structural and thermal stability upon electrochemical cycling. A micro-scale core–shell structure $Li(Ni_{0.8}Co_{0.15}Al_{0.05}O_2)_{0.8}(Ni_{0.5}Mn_{0.5})_{0.2}O_2$ (LNCANMO) was synthesized via co-precipitation. A significant improvement in the electrochemical properties and safety aspects of the core–shell structure for lithium batteries were reported compared with $LiNi_{0.8}Co_{0.15}Al_{0.05}O_2$ material.

2. Experimental

Spherical core–shell LNCANMO was synthesized as follows: spherical $Ni_{0.8}Co_{0.15}Al_{0.05}(OH)_2$ was used as the starting material (Ecopro Co. Ltd., Korea). A solution of $NiSO_4{\cdot}6H_2O$ and $MnSO_4{\cdot}H_2O$ (Ni:Mn = 1:1, molar ratio) and $Ni_{0.8}Co_{0.15}Al_{0.05}(OH)_2$ powders was continuously pumped into a reactor in N_2 atmosphere. Simultaneously, a 2.0 M NaOH solution and the desired amount of ethylene diamine solution (which acts as the chelating agent) were also pumped into the reactor. The concentration of the solutions, stirring speed (600 rpm), temperature (50 °C), reactor pH (11.4–6), and reaction time (10 h) of mixture in the reactor were all controlled carefully. The mixture in the reactor was filtered, washed, and dried to afford spherical core–shell structure $(Ni_{0.8}Co_{0.15}Al_{0.05})_{0.8}(Ni_{0.5}Mn_{0.5})_{0.2}(OH)_2$ powders. These spherical core–shell structure $(Ni_{0.8}Co_{0.15}Al_{0.05})_{0.8}(Ni_{0.5}Mn_{0.5})_{0.2}(OH)_2$ and LiOH powders, in a molar ratio of Li:(Ni + Co + Al + Mn) = 1.02:1.00, were mixed uniformly. The mixed powders were sintered at 750 °C for 3 h in oxygen atmosphere to obtain LNCANMO powders.

X-ray powder diffraction (XRD) was performed using a Rigaku ultra-X diffractometer (CuK_α radiation, 40 kV, 120 mA) in the 2θ value range of 10–80° in steps of 0.02°. The morphologies of the powders were analyzed using field emission scanning electron microscopy (FE-SEM, Supra 40, Carl Zeiss Co., Ltd.). Cross sectional images of particles were obtained by focused ion beam (FIB). The molar ratios of the metal elements present in the powders were evaluated by inductively coupled plasma (ICP, IRIS DUO, Thermo Electron Corp.) emission spectroscopy.

The electrodes were prepared by casting and pressing a mixture of 85 wt.% of the obtained material, 7.5 wt.% of KF#1300 binder (polyvinylidene difluoride: PVDF), and 7.5 wt.% of carbon black (Super P) in N-methyl pyrrolidinone (NMP) solvent on aluminum foil followed by drying for 24 h at 70 °C. The coin-type cells (CR 2016) were fabricated in an argon-filled glove box with a 1.3 M $LiPF_6$ electrolyte in an ethylene carbonate-dimethyl carbonate-ethyl methyl carbonate (EC-DMC-EMC, 3:3:4 volume ratio) solution. A Celgard 2400 film separated the positive electrode from the lithium metal negative electrode.

The cells were galvanostatically charged and discharged at a current density of 0.1–5 C in the range of 2.8–4.3 V to determine the electrochemical behavior of the cathode materials. Cyclic voltammetry (CV, Macpile biology) data of the cells were obtained at 2.7–4.8 V and at a scan rate of 0.05 mV s^{-1}. Electrochemical impedance spectroscopy (EIS) was carried out using an IVIUMSTAT. The ac perturbation signal was ±3 mV and the frequency range was from 50,000 to 0.1 Hz. The impedance spectra were analyzed using Z-View software. For differential scanning calorimetry (DSC) measurements, the Li ion cells were fully charged to 4.3 V, the positive electrode was taken out of the cell, and the electrolyte was wiped off with filter paper. A piece of crushed pellet was mechanically sealed in an aluminum cell used to collect 6–7 mg samples. The DSC signals, the heat flows (in W g^{-1}) as functions of temperature, were measured at heating rates of 10 °C min^{-1}.

3. Results and discussion

Fig. 1 shows the XRD patterns of the LNCAO and LNCANMO powders. In both cases, powders were confirmed to have a well-defined hexagonal α-$NaFeO_2$ structure with space group $R\bar{3}m$. When excess lithium was added to metal oxides containing Mn^{4+} ions, then the possibility of creating Li_2MnO_3 regions or nanodomains within a composite structure of intergrown rock salt phases exists [37]. Weak peaks (enlarged in Fig. 1a)) that are characteristic of cation ordering in the transition metal layers, as can be seen in the case of Li_2MnO_3 ($Li(Li_{1/3}Mn_{2/3})O_2$) with space group $C2/m$, are evident between $2\theta = 20°$ and 24°. This is due to approximately 10% residual lithium in the transition metal layers of the $LiNi_{0.5}Mn_{0.5}O_2$ shell (corresponding amounts of $(LiNi_{0.8}Co_{0.15}Al_{0.05})_{0.8}$ $(Li_{1.10}Ni_{0.5}Mn_{0.5})_{0.2}O_2$; Li and transition metal molar ratio of 1.02:1 in experimental process). The manganese ions are essentially all tetravalent and the nickel ions are divalent due to cation ordering of the ions [30].

Table 1 summarizes the estimated structural parameters of LNCAO and LNCANMO powders. The integrated intensity ratios (>1.25) of I_{003}/I_{104} diffraction peaks in both powders indicate excellent cation ordering. The value of I_{003}/I_{104} depends on the degree of the displacement between ions located at the 3a (Li layers) and 3b (transition metal layers) sites in a space group of $R\bar{3}m$. Thus, this value is an estimation of the reactivity of lithium insertion materials for a series of $LiNiO_2$ families. According to Ohzuku and Makimura [38], a low I_{003}/I_{104} value is an indicator of poor electrochemical reactivity due to a high concentration of inactive rock-salt domains in a layered solid matrix. The calculated lower R factors (~0.16) (defined by the intensity ratio of $I_{006}/(I_{101} + I_{012})$) for both powders also indicate excellent hexagonal ordering. Assuming a

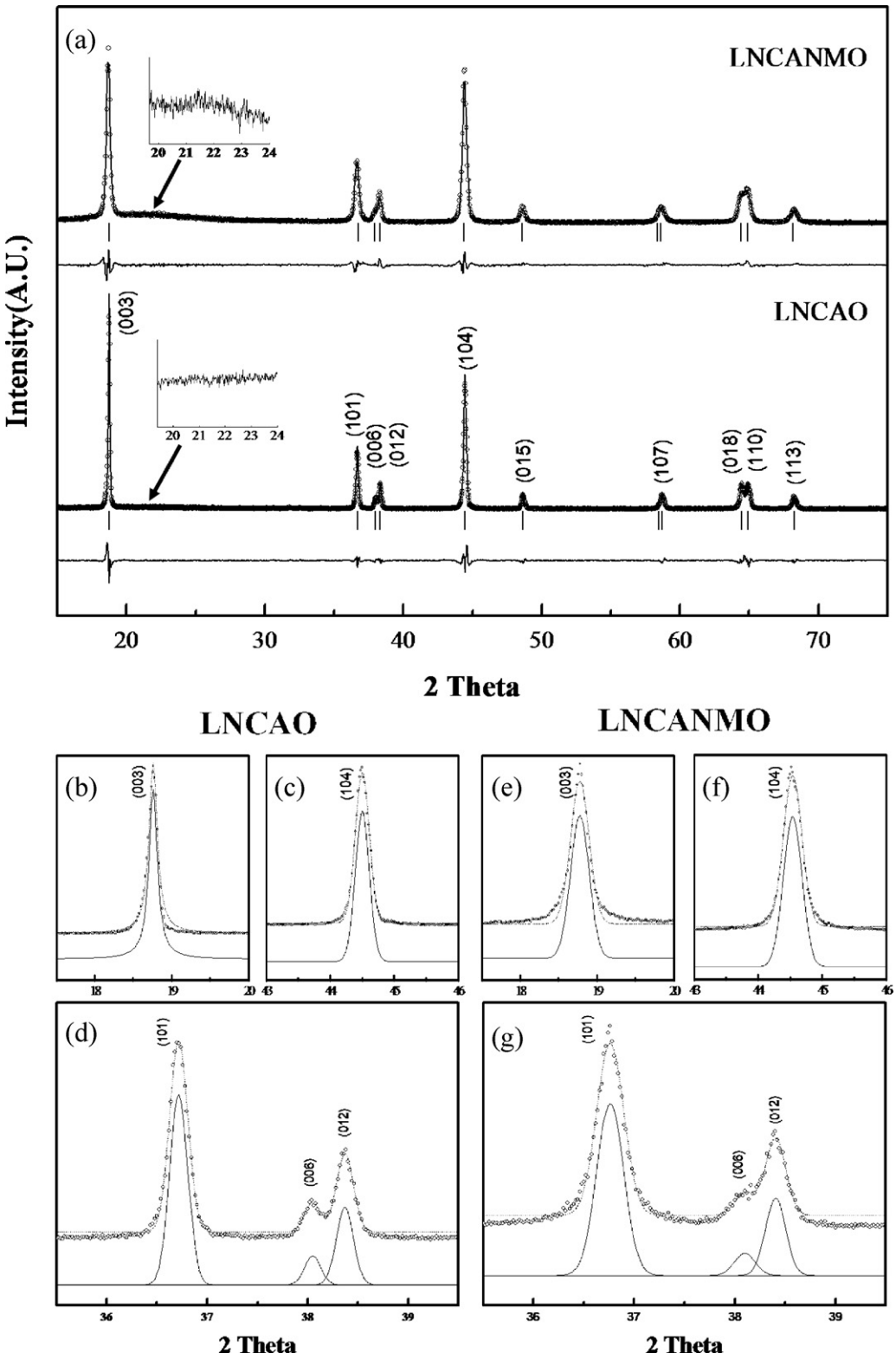

Fig. 1. (a) XRD patterns of LNCAO and LNCANMO. The difference between the observed and calculated profiles is plotted. Bragg reflections for layered oxide are indicated. XRD patterns in 20–24° 2θ regions are also shown (inset). The experimental XRD pattern (circle), fitted curve (dashed line) and the resolved peaks (solid line) for (0 0 3)/(1 0 4) and (1 0 1)/(0 0 6)/(0 1 2) peaks are shown in (b), (c), (d), (e), (f), and (g), respectively.

single phase, the lattice parameters were calculated based on the space group $R\bar{3}m$ (Table 1). The lattice parameters for the LNCANMO were somewhat higher than those of LNCAO. The lattice parameters of $LiNi_{0.5}Mn_{0.5}O_2$ have been previously reported as somewhat greater than those of LNCAO [21,27]. Therefore, it is possible that the LNCAO core surrounded by the $LiNi_{0.5}Mn_{0.5}O_2$ shell had slightly greater lattice parameters compared to LNCAO. XRD results show high hexagonal ordering and no evidence of pronounced cation mixing is observed. The electrochemical activity of these powders in terms of capacity and rates of Li deinsertion/insertion is deemed

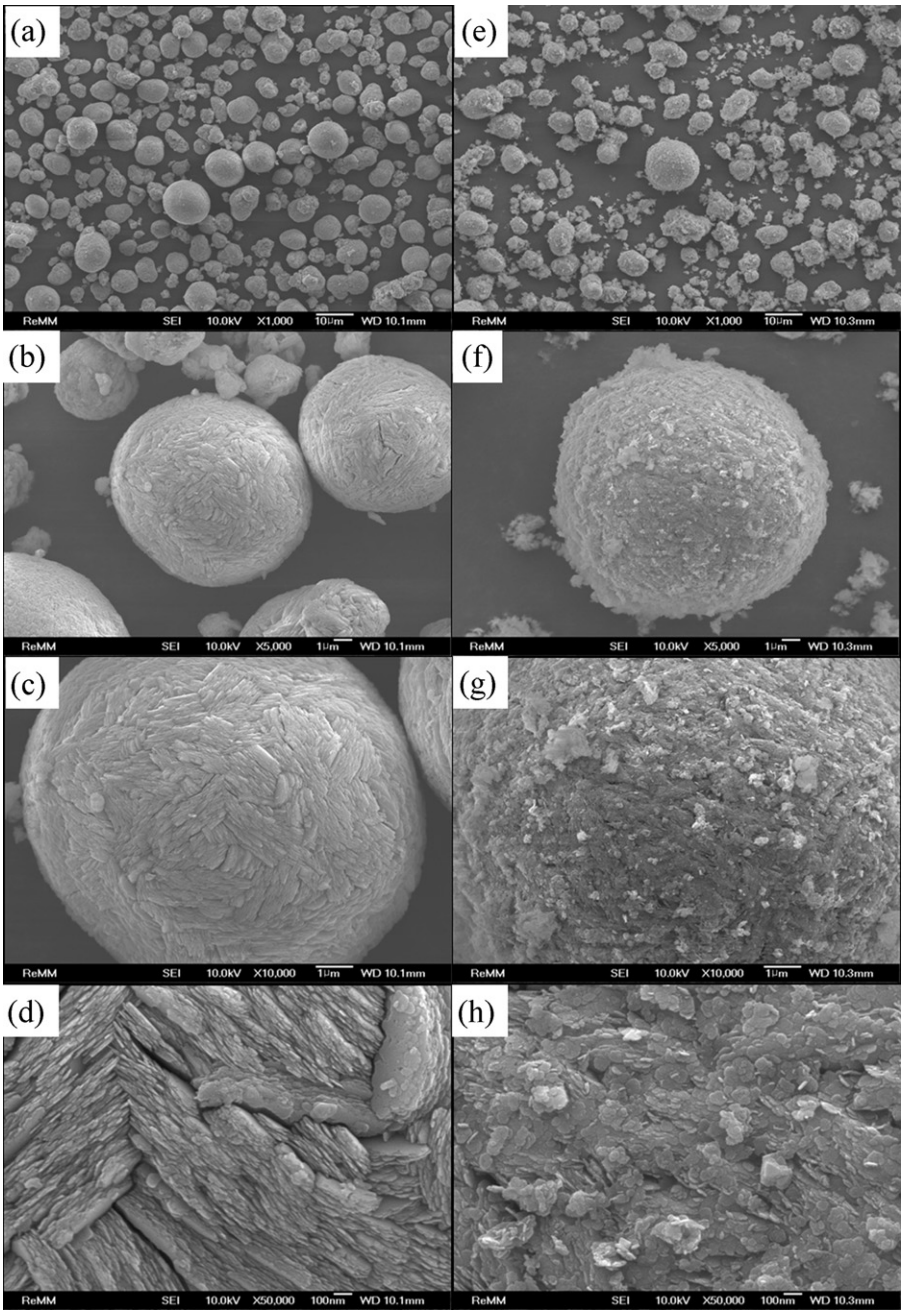

Fig. 2. FE-SEM images of (a, b, c, and d) $Ni_{0.8}Co_{0.15}Al_{0.05}(OH)_2$ and (e, f, g, and h) $(Ni_{0.8}Co_{0.15}Al_{0.05})_{0.8}(Ni_{0.5}Mn_{0.5})_{0.2}(OH)_2$.

to be very good (and comparable to results documented by Ohzuku and Makimura [38]), which is in good agreement with the results of the battery tests.

FE-SEM images of $Ni_{0.8}Co_{0.15}Al_{0.05}(OH)_2$ and $(Ni_{0.8}Co_{0.15}Al_{0.05})_{0.8}$ $(Ni_{0.5}Mn_{0.5})_{0.2}$ $(OH)_2$ are shown in Fig. 2. These two compounds consist of spherical particles. However, the surface morphology of $(Ni_{0.8}Co_{0.15}Al_{0.05})_{0.8}(Ni_{0.5}Mn_{0.5})_{0.2}(OH)_2$ is distinctly different from that of $Ni_{0.8}Co_{0.15}Al_{0.05}(OH)_2$; the surface is covered with a distributed shell of $Ni_{0.5}Mn_{0.5}(OH)_2$ (Fig. 2(f), (g), and (h)).

FE-SEM observations of the prepared LNCAO and LNCANMO illustrate that the spherical morphology of the hydroxide is maintained even after high-temperature calcinations (Fig. 3). At low magnification, both powders have similar particle sizes (~12 μm) and distributions. However, the $LiNi_{0.5}Mn_{0.5}O_2$ shell is not clearly visible on the surface of LNCAO particles, as seen in Fig. 3(f), (g), and (h). Thus, to directly verify the existence of the shell and the thickness of the synthesized LNCANMO, the powder was cut by using focused ion beam (FIB). The cross-sectional image (shown in Fig. 3(i)) clearly demonstrates the existence of the core and the shell. The thickness of the crust is approximately 1.25 μm. When compared with Fig. 2(a) and (e), it can be seen that the particle sizes before and after lithiation are almost similar.

The chemical composition of the prepared core–shell powders is $LiNi_{0.74}Co_{0.12}Mn_{0.10}Al_{0.04}O_2$, which was determined from inductively coupled plasma (ICP), and can be written as $Li(Ni_{0.8}Co_{0.15}Al_{0.05})_{0.8}(Ni_{0.5}Mn_{0.5})_{0.2}O_2$ (Table 2).

Fig. 4 shows the cyclic voltammograms for LNCAO and LNCANMO powders at room temperature in the range of 2.7–4.8 V. The scan rate was 0.05 mV s^{-1} and metallic lithium was used as the counter and reference electrodes. In general, the peaks in the CV curves correspond to the phase transitions which occur upon

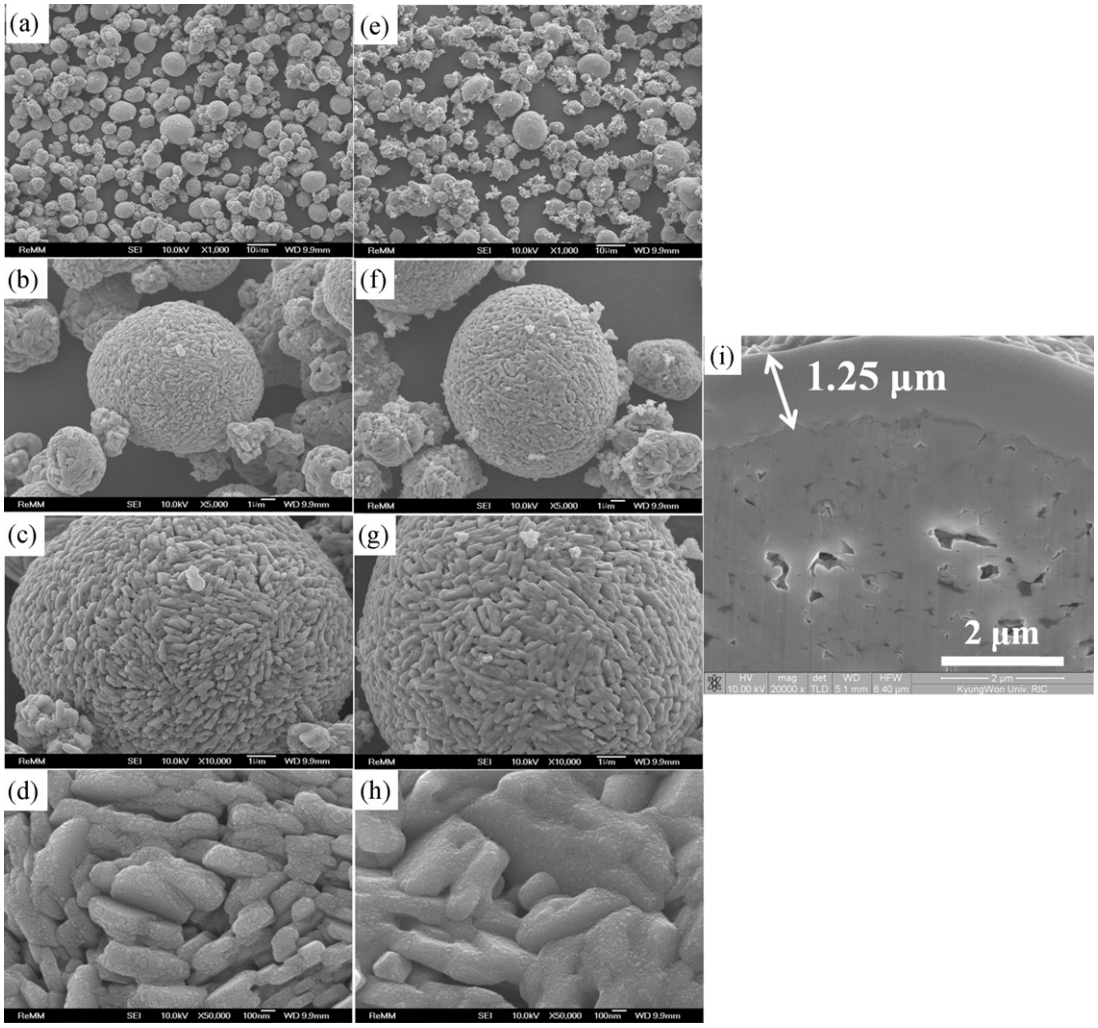

Fig. 3. FE-SEM images of (a, b, c, and d) LNCAO, (e, f, g, and h) LNCANMO, and (i) cross section image of LNCANMO core–shell.

lithium insertion and extraction. In the case of LNCAO, the first cycle oxidation peak (extraction of Li ions from the lattice) occurred at 3.93 V (versus Li), whereas the main reduction peak (insertion of Li) appeared at 3.62 V. In the second cycle, the oxidation peak shifted to a lower voltage (3.76 V), but the corresponding reduction peak was only slightly shifted (by 0.02 V) to a higher voltage. The shift in the oxidation peak voltage is an indication of the "formation" of the electrode in the first cycle, whereby the active material makes good electrical contact with the conducting carbon particles in the composite electrode, liquid electrolyte, and current collector [39]. Also, the decrease in the sharp oxidation peak area is considered to be due to the physical loss of lithium via surface film (like Li_2MO_2 [M = Co, Ni, Mn]) formation or parasitic electrochemical reactions from $LiMO_2$ during the first scan. This in turn hinders lithium re-intercalation and thus yields a large irreversible capacity in the first scan [40].

When a cathode experiences a phase transformation, a peak can be observed in the CV curve owing to the coexistence of the two phases. During charge–discharge experiments, $LiNiO_2$ exhibits four different phases (one monoclinic phase, M and three hexagonal phases, H1, H2, and H3) with three peaks apparent in the CV curve [41]. The three peaks seen for $LiNiO_2$ correspond to the coexistence of H1 and M, M and H2, and H2 and H3. $LiCoO_2$ also shows four phases (one monoclinic, M and three hexagonal, H1, H2, and H3) in the CV curve [42]. The three peaks observed for $LiCoO_2$ correspond to the coexistence of the phases H1 and H2, H2 and M, and M and H3. In this study, the positive scan of the CV curves show a sharp peak at 3.76 V and two weaker peaks at about 4.05 and 4.24 V, which cannot be clearly distinguished. The peaks represent the phase transitions of the hexagonal phase (H1) to a monoclinic phase (M) [first peak], the monoclinic phase to the second hexagonal phase (H2) [second peak], and the third peak represents the transition to

Table 2
Chemical compositions of the expected and the prepared powders.

Chemical compositions of the expected powders	Chemical compositions of the prepared powders as determined by ICP analysis
$Ni_{0.8}Co_{0.15}Al_{0.05}(OH)_2$	$Ni_{0.805}Co_{0.152}Al_{0.043}(OH)_2$
$(Ni_{0.8}Co_{0.15}Al_{0.05})_{0.8}(Mn_{0.5}Ni_{0.5})_{0.2}(OH)_2 = Ni_{0.74}Co_{0.12}Mn_{0.10}Al_{0.04}(OH)_2$	$Ni_{0.742}Co_{0.122}Mn_{0.103}Al_{0.033}(OH)_2$
$Mn_{0.5}Ni_{0.5}(OH)_2$	$Mn_{0.529}Ni_{0.471}(OH)_2$
$Li_xNi_{0.8}Co_{0.15}Al_{0.05}O_2$	$Li_xNi_{0.807}Co_{0.147}Al_{0.046}O_2$
$Li_x(Ni_{0.8}Co_{0.15}Al_{0.05})_{0.8}(Mn_{0.5}Ni_{0.5})_{0.2}O_2 = Li_xNi_{0.74}Co_{0.12}Mn_{0.10}Al_{0.04}O_2$	$Li_xNi_{0.743}Co_{0.122}Mn_{0.102}Al_{0.033}O_2$

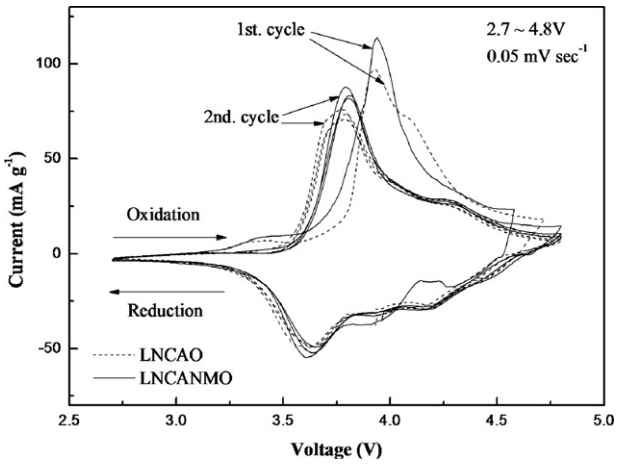

Fig. 4. Cyclic voltammograms of LNCAO and LNCANMO.

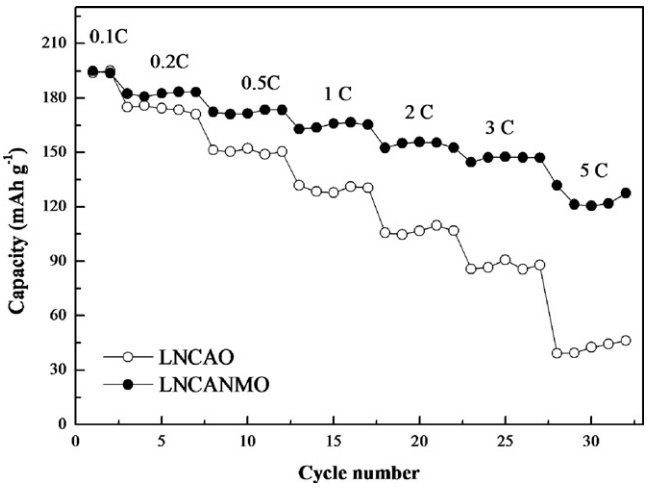

Fig. 6. Discharge profiles of LNCAO and LNCANMO cells. The cells were charged to 4.3 V with 18 mA g^{-1}(two cycles) and 36 mA g^{-1} (after two cycles) and then discharged at different rates: 18 mA g^{-1} (0.1 C), 36 mA g^{-1} (0.2 C), 90 mA g^{-1} (0.5 C), 180 mA g^{-1} (1 C), 360 mA g^{-1} (2 C), 540 mA g^{-1} (3 C), and 900 mA g^{-1} (5 C) in the 2.8–4.3 V voltage range.

the third hexagonal phase (H3) [41]. An earlier report by Han et al. describes the CV of $LiNi_{0.8}Co_{0.2}O_2$ and $LiNi_{0.8}Co_{0.15}Al_{0.05}O_2$ [8]: the second peak in the CV curve for $LiNi_{0.8}Co_{0.2}O_2$, while diminishing in intensity, merged with the first peak with increasing Al content and the first oxidation peak at 3.6 V also shifted to 3.75 V when Al was doped into $LiNi_{0.8}Co_{0.2}O_2$. The simplified CV curves and the peak shift were associated with the suppression of phase transitions due to the superior maintenance of the layered structure after doping. The CV peaks LNCAO prepared by us are similar to that of the LNCAO prepared by Han et al. [8]. In the reverse scan, the reduction peaks potentials appear at approximately 3.6, 3.9, and 4.1 V, which are symmetrical with the corresponding oxidation peaks, suggesting reversible structural changes during lithium insertion and extraction in the LNCAO powders. The CV of LNCANMO is almost identical to that of LNCAO. However, the second cycle oxidation peak occurs at a higher voltage (3.81 V) than that of pristine LNCAO (3.76 V). No redox peaks can be seen at around 3 V in the CV curve, indicating that the Mn ion is electrochemically inactive and present in the 4+ oxidation state in the $LiNi_{0.5}Mn_{0.5}O_2$ shell. Two major peaks at 4.0 and 3.6 V for the Li/$LiNi_{0.5}Mn_{0.5}O_2$ cell were reported by Lu et al. and Kang et al. [43,44]. These are at a higher voltage than that of LNCAO. The observed shift in the oxidation peak to at higher voltage may be attributed to $LiNi_{0.5}Mn_{0.5}O_2$ shell.

Fig. 5 shows the charge–discharge profiles of the LNCAO and LNCANMO powders during the first cycle. The first-charge capacity of LNCAO is 230 mAh g^{-1} (LNCANMO is 236 mAh g^{-1}) and the first-discharge capacity is 200 mAh g^{-1}. Hence, the irreversible capacity loss (ICL) in the first cycle is >30 mAh g^{-1}, which is believed to be the formation of a Li_2MO_2-like phase on the oxide particle surface because lithium diffusion in $Li_{1-\Delta}MO_2$ with $\Delta \rightarrow 0$ (i.e., near the end of discharge) is very sluggish [40]. These results are compliant with those of the CV analysis. Also, both powders show good electrochemical activity with high initial discharge capacity due to their outstanding crystallinity.

Fig. 6 shows the discharge profiles for the LNCAO and LNCANMO cells at various C-rates (18[0.1 C] ~ 900[5 C] mA g^{-1}) between 2.8 and 4.3 V. It is clear that the LNCANMO cell has improved capacity retention over the tested C-rate range. For example, LNCANMO shows capacity retentions of 85.1% and 65.1% at rates of 1 and 5 C, respectively, compared to the corresponding values of 67.2% and 21.6% for LNCAO. The comparison of cycling performance for the prepared LNCAO and LNCANMO materials is displayed in Fig. 7. The cells were cycled at a constant current of 18 mA g^{-1} in the voltage range of 2.8–4.3 V. The cycling behavior of the LNCANMO is quite stable showing good capacity retention. From these results (Figs. 6 and 7), the improved capacity retention of the LNCANMO material probably results from the existence of the shell mate-

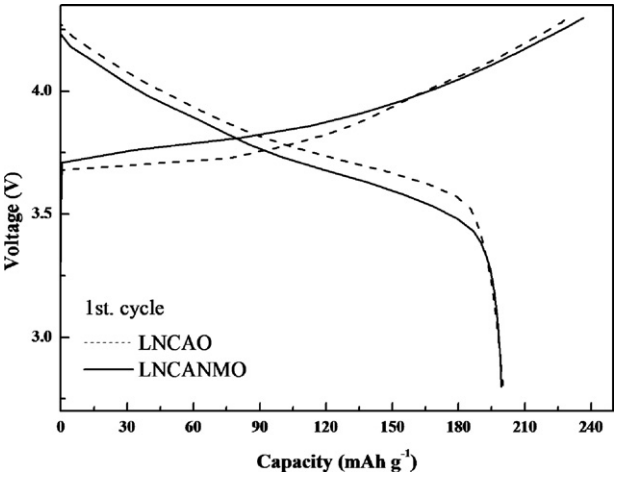

Fig. 5. First charge–discharge curves of LNCAO and LNCANMO cells at a current density of 18 mA g^{-1}(0.1 C) in 2.8–4.3 V.

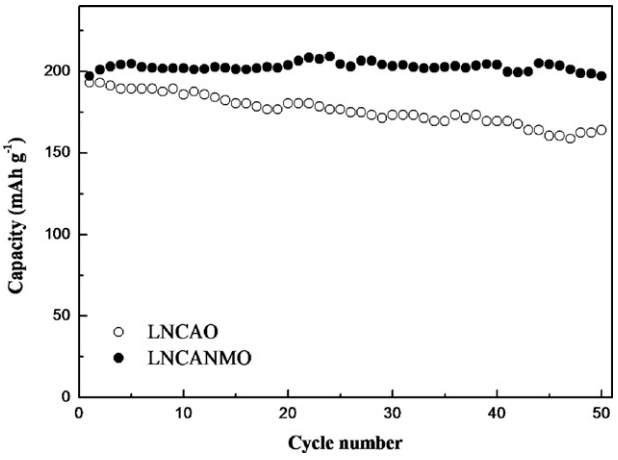

Fig. 7. Cyclic performance of LNCAO and LNCANMO cells at a current density of 18 mA g^{-1} (0.1 C) in 2.8–4.3 V voltage range.

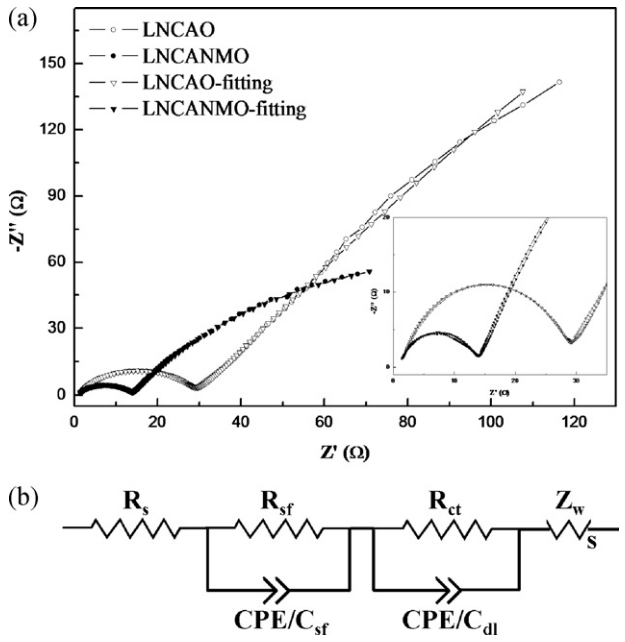

Fig. 8. Nyquist plots of LNCAO and LNCANMO electrode materials at first cycled state (4.3–2.8 V): (a) experimental results vs. fitted plots and (b) equivalent circuit model. Magnification of the plots in high-frequency regions is also shown (inset).

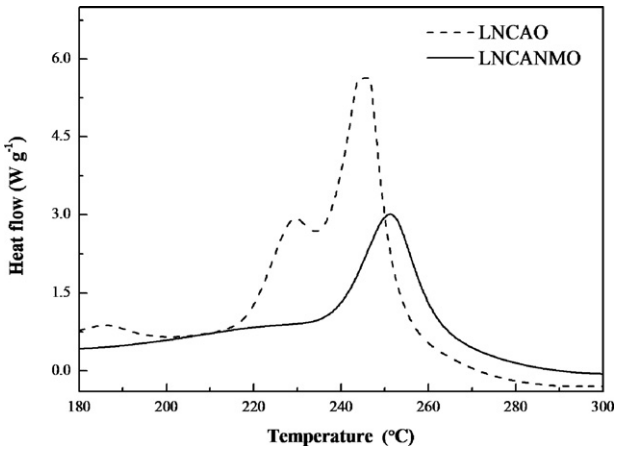

Fig. 9. Differential scanning calorimetry profiles of LNCAO and LNCANMO after charge state until 4.3 V.

rial, which is consistent with the XRD and EIS analysis. However, although LNCAO has high initial discharge capacity with good crystallinity, $LiNiO_2$ and its derivatives $LiNi_{1-x}Co_xO_2$ suffer from structural instability caused by structural deformation especially when cycled above 4.3 V. Furthermore, Co dissolution induced by HF generated from the electrolyte in the presence of H_2O leads to deterioration of the $LiNi_{1-x}Co_xO_2$ type material [45]. Thus, as the cycle progresses, LNCAO exhibits the poor charge–discharge performance. Since the LNCAO core is surrounded by structurally stable $LiNi_{0.5}Mn_{0.5}O_2$ shell, the possibility of HF attack to the LNCAO in the electrolyte solution should be prevented during the cycling. In addition, Co dissolution should be suppressed. Furthermore, the amount of Li_2MO_2 covering on the surface of LNCAMNO might be lower than the levels of Li_2MO_2 on LNCAO. The production of surface film (Li_2MO_2) on the electrode will be discussed when describing EIS analysis. Additionally, the $LiNi_{0.5}Mn_{0.5}O_2$ (shell) is known to have a stable cycling performance due to its electrochemical structure and associated small changes in cell volume [33,46]. Therefore, its discharge capacity during the cycling is maintained as shown in Figs. 6 and 7.

Electrochemical impedance spectroscopy (EIS) is a powerful tool to probe the kinetics of lithium intercalation/deintercalation into electrodes [47,48]. The lithium intercalation and deintercalation into the cathode materials can be modeled as a multi-step process that involves and reflects the serial nature of several processes occurring during intercalation/deintercalation. The general nature of these models is to explain the Li-ion migration through the surface film, charge-transfer through the electrode/electrolyte interface, and the solid-state diffusion of Li in the compounds. The impedance plots were fitted using an equivalent circuit model (Fig. 8(b)), and the fitted impedance parameters are listed in Table 3.

Table 3
The obtained parameters from simulation of elements in equivalent circuit model.

Samples	R_s (Ω)	R_{sf} (Ω)	R_{ct} (Ω)
LNCAO	1.2	26.33	1890
LNCANMO	0.9	12.65	180.1

The experimentally visualized processes that are possible are (1) a resistive component (R_s) arising from the electrolyte resistance and cell components, (2) the double layer (dl) capacitance of the surface film and the associated impedance (C_{sf} and R_{sf}), (3) the charge transfer (electron transfer) resistance of the intercalation reaction and the capacitance of the double layer (R_{ct} and C_{dl}), and (4) a Warburg impedance (Z_W) which is characteristic of the Li ion diffusion through the bulk to the active material [48].

EIS tests were performed on the electrodes at the first cycle, which is charged in the range of 4.3–2.8 V. In Fig. 8(a), two semicircles denote the endpoint of deintercalation and intercalation. The electrode kinetics is controlled by the charge transfer contribution [49]. In general, the low-frequency semicircle contains the contribution of contact impedance between inter-particles [50,51]. The diameter of which, in the plots of the electrode, provides charge-transfer resistance (R_{ct}) associated with the electrochemical process. Using the equivalent circuit, the R_{ct} of LNCAO (1890 Ω) is larger than LNCANMO (180.1 Ω). The high frequency semicircle may be attributed to the charge transfer process in the electrode/electrolyte interface, namely, the change of the high-frequency semicircle size may reflect the growth of a passive surface film formed by the reaction between the lithium metal oxide and electrolyte [50,51]. In the inset magnification shown in Fig. 8(a), the sizes of the low-frequency semicircles have the same variation as that at low frequency, indicating that LNCAO has a larger surface film resistance (R_{sf}) at the first cycle. The R_{sf} may not have a significant role in the electrode kinetics for a single charge or discharge cycle. However, the production of surface film, which may be Li_2MO_2 formation or parasitic electrochemical reactions, on the electrode in case of repeating charge–discharge cycling may influence the performance of the electrode material. The nature of surface film, which covers the active mass, may provide a measure of its particle-to-particle contact. A mass deposition of the surface film on the electrode surface may end up being destructive film, which can slow down the electrode kinetics and hence impair its performance [47,52,53]. Thus, the poor charge–discharge performance of LNCAO material may be attributed to the higher charge transfer resistance coupled with the surface film resistance, and the observed higher current rate capability and cycle stability of LNCANMO can explained by the lower surface film resistance and charge transfer resistance.

Differential scanning calorimetry was performed in order to compare the thermal stability of the LNCAO and LNCANMO powders, especially in the charged 4.3 V state (Fig. 9). The exothermic peak area indicates the level of heat generation (related to oxygen generation) of the decomposed cathode after reac-

tion with the electrolyte. $Li_{1-x}(Ni_{0.8}Co_{0.15}Al_{0.05})O_2$ has a large exothermic peak at 245 °C, the onset of decomposition occur at 214 °C, and the reaction releases 740 J g^{-1} of heat. However, $Li_{1-x}(Ni_{0.8}Co_{0.15}Al_{0.05})_{0.8}(Ni_{0.5}Mn_{0.5})_{0.2}O_2$ shows a higher temperature (251 °C between 235 °C and 270 °C) with a much lower amount of exothermic heat release (350 J g^{-1}). The improved thermal stability of $Li_{1-x}(Ni_{0.8}Co_{0.15}Al_{0.05})_{0.8}(Ni_{0.5}Mn_{0.5})_{0.2}O_2$ may be attributed to the thermally stable $LiNi_{0.5}Mn_{0.5}O_2$ shell [31], which suppresses the oxygen release from the host lattice. The thermally stable $LiNi_{0.5}Mn_{0.5}O_2$ shell encapsulating the core material also serves to improve the overall stability. Thus, the thermally instable $Li_{1-x}(Ni_{0.8}Co_{0.15}Al_{0.05})O_2$ [21] core did not come into direct contact with the electrolyte solution. LNCANMO provides better thermal stability in the charged state.

4. Conclusions

We synthesized the cathode material $Li(Ni_{0.8}Co_{0.15}Al_{0.05})_{0.8}(Ni_{0.5}Mn_{0.5})_{0.2}O_2$ (LNCANMO) with core–shell structure using a co-precipitation method. The capacity retention is significantly improved relative to that of the $Li(Ni_{0.8}Co_{0.15}Al_{0.05})O_2$ (LNCAO) electrode without the $LiNi_{0.5}Mn_{0.5}O_2$ shell. Because the LNCAO core is surrounded by structurally stable $LiNi_{0.5}Mn_{0.5}O_2$ as shell, it should prevent the possibility of HF attack on LNCAO in the electrolyte solution during the cycling. In addition, Co dissolution should be suppressed. Using the equivalent circuit model, the R_{ct} and R_{sf} of LNCAO are larger than that of LNCANMO, and thus exhibit poorer electrochemical performance. However, the LNCANMO possesses higher current rate capability and cycle stability owing to its better charge transfer kinetics and lower surface film resistance. Also, the thermal stability of the fully charged LNCANMO is slightly better than that of LNCAO, as confirmed by the DSC. The improved thermal stability of the $Li_{1-x}(Ni_{0.8}Co_{0.15}Al_{0.05})_{0.8}(Ni_{0.5}Mn_{0.5})_{0.2}O_2$ is due to the thermally stable outer $LiNi_{0.5}Mn_{0.5}O_2$ shell, which suppresses oxygen release from the host lattice. In addition, the thermally stable outer $LiNi_{0.5}Mn_{0.5}O_2$ shell encapsulates the core material, and so that the thermally instable $Li_{1-x}(Ni_{0.8}Co_{0.15}Al_{0.05})O_2$ core does not come into direct contact with electrolyte solution. LNCANMO has improved electrochemical properties as an electrode for lithium-ion batteries.

Acknowledgment

This work was supported by Priority Research Centers Program through the National Research Foundation of Korea (NRF) funded by the Ministry of Education, Science and Technology (2009-0093818) and from the World Class University (WCU) program (R33-2008-000-10003).

References

[1] T. Ohzuku, A. Ueda, M. Nagayama, J. Electrochem. Soc. 140 (1993) 1862–1870.
[2] J.R. Dahn, E.W. Fuller, M. Obrovac, U. von Sacken, Solid State Ionics 69 (1994) 265–270.
[3] H. Arai, M. Tsuda, K. Saito, M. Hayashi, Y. Sakurai, J. Electrochem. Soc. 149 (2002) A401–A406.
[4] I. Saadoune, C. Delmas, J. Solid State Chem. 136 (1998) 8–15.
[5] A.G. Ritchie, C.O. Gowa, J.-C. Lee, P. Bowles, A. Gilmour, J. Allen, D.A. Rice, F. Brady, S.C.E. Tsang, J. Power Sources 80 (1999) 98–102.
[6] D. Caurant, N. Baffler, B. Carcia, J.P. Pereira-Ramos, Solid State Ionics 91 (1996) 45–54.
[7] H. Cao, B. Xia, N. Xu, C. Zhang, J. Alloy Compd. 376 (2004) 282–286.
[8] C.J. Han, J.H. Yoon, W.I. Cho, H. Jang, J. Power Sources 136 (2004) 132–138.
[9] G.T.K. Fey, H.Z. Yang, T.P. Kumar, Ionics 9 (2003) 182–188.
[10] S.C. Park, Y.S. Han, P.S. Lee, S.H. Ahn, H.M. Lee, J.Y. Lee, J. Power Sources 102 (2001) 130–134.
[11] C.J. Han, W. Eom, S. Lee, W.I. Cho, H. Jang, J. Power Sources 144 (2005) 214–219.
[12] J. Xiang, C. Chang, F. Zhang, J. Sun, J. Alloy Compd. 475 (2009) 483–487.
[13] X. Ma, C. Wang, J. Cheng, J. Sun, Solid State Ionics 178 (2007) 125–129.
[14] G.T.K. Fey, V. Subramanian, J.G. Chen, Mater. Lett. 52 (2002) 197–202.
[15] H. Liu, J. Li, Z. Zhang, Z. Gong, Y. Yang, Electrochim. Acta 49 (2004) 1151–1159.
[16] G.T.K. Fey, J.G. Chen, V. Subramanian, T. Osaka, J. Power Sources 112 (2002) 384–394.
[17] K.K. Lee, W.S. Yoon, K.B. Kim, K.Y. Lee, S.T. Hong, J. Power Sources 97–98 (2001) 308–312.
[18] M. Guilmard, L. Croguennec, D. Denux, C. Delmas, Chem. Mater. 15 (2003) 4476–4483.
[19] S.H. Yoon, C.W. Lee, Y.S. Bae, I.K. Hwang, Y.K. Park, J.H. Song, Electrochem. Solid-State Lett. 12 (2009) A211–A214.
[20] H.B. Kim, B.C. Park, S.T. Myung, K. Amine, J. Prakash, Y.K. Sun, J. Power Sources 179 (2008) 347–350.
[21] I. Belharouak, W. Lu, D. Vissers, K. Amine, Electrochem. Commun. 8 (2006) 329–335.
[22] T. Ohzuku, Y. Makimura, Chem. Lett. (2001) 744–745.
[23] S.H. Choi, O.A. Shlyakhtin, J. Kim, Y.S. Yoon, J. Power Sources 140 (2005) 355–360.
[24] H. Xia, S.B. Tang, L. Lu, J. Alloy Compd. 449 (2008) 296–299.
[25] M. Yoncheva, R. Stoyanova, E. Zhecheva, R. Alcántara, J.L. Tirado, J. Alloy Compd. 475 (2009) 96–101.
[26] W.S. Yoon, C.P. Grey, M. Balasubramanian, X.Q. Yang, J. McBreen, Chem. Mater. 15 (2003) 3161–3169.
[27] C.S. Johnson, J.S. Kim, A.J. Kropf, A.J. Kahaian, J.T. Vaughey, L.M.L. Fransson, K. Edstrom, M.M. Thackeray, Chem. Mater. 15 (2003) 2313–2322.
[28] Y. Koyama, Y. Makimura, I. Tanaka, H. Adachi, T.J. Ohzuku, J. Electrochem. Soc. 151 (2004) A1499–A1506.
[29] J. Reed, G. Ceder, Electrochem. Solid State Lett. 5 (2002) A145–148.
[30] A. Deb, U. Bergmann, S.P. Cramer, E.J. Cairns, J. Appl. Phys. 99 (2006) 063701.
[31] S.H. Kang, K.J. Amine, J. Power Sources 119–121 (2003) 150–155.
[32] S.T. Myung, S. Komaba, K. Kurihara, K. Hosoya, N. Kumagai, Y.K. Sun, I. Nakai, M. Yonemura, T. Kamiyama, Chem. Mater. 18 (2006) 1658–1666.
[33] X.Q. Yang, J. McBreen, Y.S. Yoon, C.P. Grey, Electrochem. Commun. 4 (2002) 649–654.
[34] Y.K. Sun, S.T. Myung, M.H. Kim, J. Prakash, K. Amine, J. Am. Chem. Soc. 127 (2005) 13411–13418.
[35] Y.K. Sun, S.T. Myung, H.S. Shin, Y.C. Bae, C.S. Yoon, J. Phys. Chem. B 110 (2006) 6810–6815.
[36] K.S. Lee, S.T. Myung, Y.K. Sun, J. Power Sources 195 (2010) 6043–6048.
[37] M.M. Thackeray, S.H. Kang, C.S. Johnson, J.T. Vaughey, S.A. Hackney, Electrochem. Commun. 8 (2006) 1531–1538.
[38] Y. Makimura, T. Ohzuku, J. Power Sources 119–121 (2003) 156–160.
[39] K.S. Tan, M.V. Reddy, G.V.S. Rao, B.V.R. Chowdari, J. Power Sources 141 (2005) 129–142.
[40] S.H. Kang, D.P. Abraham, W.S. Yoon, K.W. Nam, X.Q. Yang, Electrochim. Acta 54 (2008) 684–689.
[41] W. Li, J.N. Reimers, J.R. Dahn, Solid State Ionics 67 (1993) 123–130.
[42] J.N. Reimers, J.R. Dhan, J. Electrochem. Soc. 139 (1992) 2091–2097.
[43] Z.H. Lu, L.Y. Beaulileu, R.A. Donaberger, C.L. Thomas, J.R. Dahn, J. Electrochem. Soc. 149 (2002) A778–A791.
[44] S.H. Kang, J. Kim, M.E. Stoll, D. Abraham, Y.K. Sun, K. Amine, J. Power Sources 112 (2002) 41–48.
[45] G.G. Amatucci, M.M. Tarascon, L.C. Klein, Solid State Ionics 83 (1996) 167–173.
[46] K.S. Lee, S.T. Myung, J.S. Moon, Y.K. Sun, Electrochim. Acta 53 (2008) 6033–6037.
[47] M.D. Levi, K. Gamolsky, D. Aurbach, U. Heider, R. Oesten, Electrochim. Acta 45 (2000) 1781–1789.
[48] K.M. Shaju, G.V. Subba Rao, B.V.R. Chowdari, J. Electrochem. Soc. 150 (2003) A1–A13.
[49] X. Meng, S. Dou, W.L. Wang, J. Power Sources 184 (2008) 489–493.
[50] M.D. Levi, G. Salitra, B. Markovsky, H. Teller, D. Aurbach, U. Heider, L. Heider, J. Electrochem. Soc. 146 (1999) 1279–1289.
[51] K.A. Striebel, E. Sakai, E.J. Cairns, J. Electrochem. Soc. 149 (2002) A61–A68.
[52] A. Ueda, T. Ohzuku, J. Electrochem. Soc. 141 (1994) 2010–2014.
[53] N. Yabuuchi, T. Ohzuku, J. Power Sources 119–121 (2003) 171–174.